Molecular Cancer Therapeutics

Basal-A Triple-Negative Breast Cancer Cells Selectively Rely on RNA Splicing for Survival

Stefanie Chan[1,2], Praveen Sridhar[1,2], Rory Kirchner[3], Ying Jie Lock[1,2], Zach Herbert[4], Silvia Buonamici[5], Peter Smith[5], Judy Lieberman[6], and Fabio Petrocca[1,2]

Abstract

Prognosis of triple-negative breast cancer (TNBC) remains poor. To identify shared and selective vulnerabilities of basal-like TNBC, the most common TNBC subtype, a directed siRNA lethality screen was performed in 7 human breast cancer cell lines, focusing on 154 previously identified dependency genes of 1 TNBC line. Thirty common dependency genes were identified, including multiple proteasome and RNA splicing genes, especially those associated with the U4/U6.U5 tri-snRNP complex (e.g., *PRPF8*, *PRPF38A*). *PRPF8* or *PRPF38A* knockdown or the splicing modulator E7107 led to widespread intronic retention and altered splicing of transcripts involved in multiple basal-like TNBC dependencies, including protein homeostasis, mitosis, and apoptosis. E7107 treatment suppressed the growth of basal-A TNBC cell line and patient-derived basal-like TNBC xenografts at a well-tolerated dose. The antitumor response was enhanced by adding the proteasome inhibitor bortezomib. Thus, inhibiting both splicing and the proteasome might be an effective approach for treating basal-like TNBC. *Mol Cancer Ther; 16(12); 2849–61. ©2017 AACR.*

Introduction

Triple-negative breast cancers (TNBC), defined by their lack of estrogen (ER), progesterone, and HER2 receptors, are a heterogeneous group of poorly differentiated and aggressive tumors that disproportionately affect younger and African American women (1–3). TNBCs are classically defined as "basal-like" or "claudin-low" based on gene expression. Basal-like tumors (the most common variant) display a luminal/myoepithelial or progenitor-like phenotype, whereas claudin-low tumors express predominantly mesenchymal traits. mRNA expression analysis further divides TNBC into six molecular subtypes, which are basal-like (BL-1, BL-2, IM), claudin-low (M, MSL), or molecular apocrine tumors (LAR; ref. 4). Basal-A and basal-B breast cancer cell lines resemble basal-like and claudin-low tumors, respectively (5). Genome sequencing corroborates TNBC diversity; apart from *TP53* mutations, which occur in >80% of TNBCs, no recurrent genetic lesions that could serve as drug targets have been identified (6–8).

To identify novel TNBC therapeutic targets, we previously performed a genome-wide siRNA lethality screen to identify selective basal-like TNBC genetic dependencies by comparing a pair of isogenic, genetically well-defined TNBC cell lines, basal-A BPLER, and myoepithelial HMLER (9). The screen identified 154 genes selectively needed for BPLER survival. *MCL1* and multiple proteasome genes scored as top BPLER dependency genes and as shared dependencies of basal-A cell lines. Basal-A cell lines were selectively sensitive to the proteasome inhibitor drug bortezomib. Proteasome addiction was linked to Mcl-1 dependence. However, the MTD of bortezomib was needed for an effective antitumor response, which may explain the failure of bortezomib in clinical trials in TNBC.

Because of TNBC heterogeneity and the inadequacy of current treatment, here we sought to identify additional shared genetic dependencies that might be useful TNBC drug targets. To this end, we performed a targeted siRNA lethality screen using 4 basal-A and 3 luminal human cell lines, focusing on the 154 BPLER dependency genes. Knockdown of only 30 genes resulted in at least a mean 2-fold loss in viability of the 4 TNBC lines. These included *MCL1* and 5 genes linked to the proteasome, confirming our earlier work (9). mRNA splicing genes were prominent basal-A shared dependencies, comprising 12 of the remaining 24 hits. These results confirm other studies that identified splicing as a selective TNBC dependency (10–12). Over 200 proteins assemble with small nuclear RNAs (snRNA) to form multiple small nuclear ribonucleoprotein (snRNP) complexes that control distinct steps of splicing (13). Four of the 12 splicing gene hits are either components of the U4/U6.U5 tri-snRNP complex (*PRPF6*, *PRPF8*, *PRPF38A*) or associated with it (*USP39*). The tri-snRNP complex plays a key early role in splicing—it associates with the initial spliceosome A complex to form the B complex to promote the catalytic activation of the spliceosome (14–17). More differentiated luminal breast cancer cell lines were not as dependent on

[1]Division of Computational Biomedicine, Department of Surgery, Boston University School of Medicine, Boston, Massachusetts. [2]Division of Computational Biomedicine, Department of Medicine, Boston University School of Medicine, Boston, Massachusetts. [3]Bioinformatics Core, Harvard T.H. Chan School of Public Health, Boston, Massachusetts. [4]Molecular Biology Core Facilities, Dana-Farber Cancer Institute, Boston, Massachusetts. [5]H3 Biomedicine Inc., Cambridge, Massachusetts. [6]Program in Cellular and Molecular Medicine, Boston Children's Hospital and Department of Pediatrics, Harvard Medical School, Boston, Massachusetts.

Note: Supplementary data for this article are available at Molecular Cancer Therapeutics Online (http://mct.aacrjournals.org/).

S. Chan and P. Sridhar contributed equally to this article.

Corresponding Authors: Fabio Petrocca, Boston University School of Medicine, 700 Albany Street, Boston, MA 02118. Phone: 614-218-2940; Fax: 617-638-8665; E-mail: fabio.petrocca@gmail.com; and Judy Lieberman, judy.lieberman@childrens.harvard.edu

doi: 10.1158/1535-7163.MCT-17-0461

these splicing genes, suggesting that transient inhibition of splicing might be well-tolerated by normal cells. Because of the overrepresentation of hits in this functionally important complex, we focused on these splicing hits in this study.

Materials and Methods

Cell lines

HCC70, HCC1143, HCC1187, HCC1937, HCC1954, HCC1806, AU565, BT474, MCF7, MDAMB231, MDAMB436, and BT549 cell lines were purchased directly from ATCC. The MB468 cell line was engineered to express luciferase and was obtained from Dr. A. Kung (Memorial Sloan Kettering Cancer Center). All cell lines were tested for Mycoplasma infection by PCR every 3 months. Only early-passage cell lines were used, and cells were kept in culture no longer than 21 days. Cell lines were obtained in 2012 with the exception of MDAMB231 that was obtained in 2016. Cell lines were authenticated by short tandem repeat analysis. Bortezomib was purchased from LC Laboratories. E7107 (18) was kindly provided by H3 Biomedicine, Inc.

High-throughput screening

Automated siRNA screening was performed using robotics at the ICCB-L Screening Facility at Harvard Medical School, as previously described (9). Briefly, high-throughput screening (HTS) conditions optimized in our previous study were tested in 22 human breast cancer cell lines, and cell lines showing a Z′ factor > 0.6 were selected for targeted screening using a customized 252 siRNA library of validated siRNAs (siGenome; Dharmacon) against the 154 BPLER dependency genes identified in ref. 9. Cells (1,000/well) were reverse-transfected with individual siRNAs (50 nmol/L) in triplicate in 384-well flat clear-bottom white polystyrene microplates (Corning) using Dharmafect 1 (0.04 μL/well) and a 1:1 mixture of Optimem/10% FBS RPMI 1640 medium (final volume: 25 μL/well). Fresh 10% FBS RPMI 1640 (15 μL/well) was added 24 hours after transfection, and cell viability was measured by CellTiterGlo chemoluminescence assay (Promega) 72 hours after transfection using an Infinite M100 Pro high-throughput plate reader (Tecan), after verifying that the detected signal was within a linear range. For each siRNA, the viability scores of the three replicates were averaged and compared with the average score of cells transfected with a control siRNA with no detectable effect on viability (Non-targeting Control #4; Dharmacon). The heatmap of cell viability ratios was generated using the Gplot2 package within R.

RNA library preparation and sequencing

Libraries were prepared using Illumina TruSeq Stranded mRNA sample preparation kits from 500 ng of purified total RNA according to the manufacturer's protocol. The finished dsDNA libraries were quantified by Qubit fluorometer, Agilent TapeStation 2200, and qRT-PCR using the Kapa Biosystems library quantification Kit according to the manufacturer's protocols. Uniquely indexed libraries were pooled in equimolar ratios and sequenced on two Illumina NextSeq500 runs with paired-end 75 bp reads at the Dana-Farber Cancer Institute Molecular Biology Core Facilities.

RNA-seq data analysis

Raw RNA-seq data were deposited in the GEO database (GSE90519). All of the analysis scripts to reproduce the analysis are stored in the Github repository and are accessible online (19). A step-by-step description of data analysis procedures is also available online (20). Pathway analyses were based on the Reactome web-based tool within the Molecular Signatures Database (MSigDB) of the Broad Institute (21) using a cut-off of $q < 0.05$. Gene networks were generated using GeneMania (22) focusing on physical interactions, pathway, and shared protein domain interactions.

Protein analysis

Immunoblot was performed as previously described (9). Briefly, cells were lysed in 1X Cell Lysis Buffer (Cell Signaling Technology), and 30 to 50 μg of total proteins were boiled for 5 minutes in 1X NuPage buffer + DTT (Life Technologies), resolved on a 4%–20% Tris-HCl polyacrylamide gradient Criterion gel (Biorad) and transferred to a PVDF membrane using a Criterion wet-transfer system (Biorad) for 3 hours at 0.35 A. A list of antibodies used is shown in Supplementary Materials and Methods.

qRT-PCR and RT-PCR

Total RNA was extracted from pelleted cells using the RNeasy Plus Mini Kit (Qiagen; Cat# 74134). First strand cDNA synthesis was performed using the iScript cDNA synthesis Kit (BioRad; Cat# 1708891) using 1 μg of total RNA and following the manufacturer's protocol.

Mouse studies

Animal experiments involving cell line–derived xenografts were performed in the Association for Assessment and Accreditation of Laboratory Animal Care International (AAALAC)-accredited Laboratory Animal Science Center at Boston University Medical Campus. All experiments were conducted in accordance with Boston University's Institutional Animal Care and Use Committee. Approximately 6-week-old, female, nude mice (NU/J; Jackson Laboratory) were used. Briefly, for each mouse, 3×10^6 or 1×10^7 HCC1187 cells or 2×10^6 MB468 cells were injected subcutaneously in the right flank in a 1:1 solution of Matrigel (BD Bioscience) and 10% FBS RPMI 1640 using 26G needles, in a final volume of 100 μL. When tumors were palpable (usually within ∼4–6 weeks), mice were randomized into groups with tumors of similar size (50 ± 10 mm^3) and treated by tail-vein injection with 5 mg/kg E7107, 0.4 to 1.2 mg/kg bortezomib, or vehicle (DMSO) in 100 μL volume in PBS once a day for 4 or 5 consecutive days. Tumor volume was measured every 2 or 3 days by caliper, and statistical significance was determined by one-sided t test. Patient-derived xenograft (PDX)–based experiments were conducted in collaboration with Champions Oncology Inc. based on a comparable protocol, with the exception that Ncr nude mice (Taconic) were used instead of NU/J. Each of the models was previously validated by histopathology and characterized by RNA-seq and whole-exome sequencing. Data are available on the Champions Oncology website (23).

Results

A targeted siRNA screen identifies core survival networks in basal-A breast cancer cell lines

Seventy-seven percent of the 154 BPLER dependency genes (9) clustered within 13 well-defined gene networks that control key

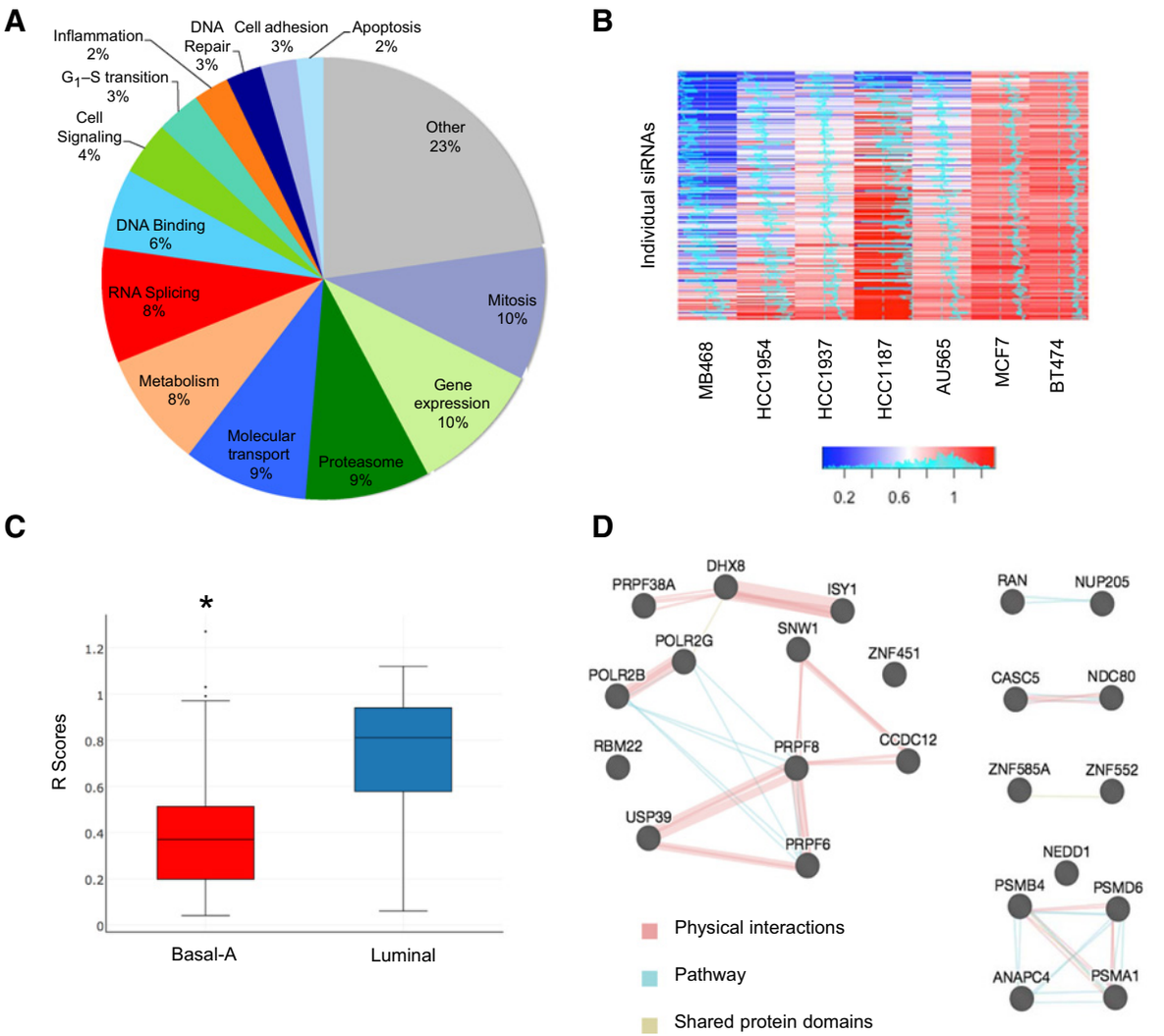

Figure 1.

A targeted siRNA screen identifies shared vulnerabilities of basal-A TNBC versus luminal breast cancer cell lines. **A,** Distribution of pathway assignments of the 252 siRNAs used in this screen. **B,** Viability heatmap of the indicated cell lines 72 hours after transfection with individual siRNAs targeting the 154 BPLER dependency genes, relative to transfection with a nontargeting siRNA. Histograms in heatmap indicate score distance from 0.5 (midline). Histogram in color key indicates counts of specific scores across all cell lines. MB468, HCC1954, HCC1937, and HCC1187 cell lines are basal-A; AU565, MCF7, and BT474 are luminal. **C,** Box–whisker plot showing the distribution of *R* scores associated with the genes in Supplementary Table S2 in basal-A versus luminal cell lines. *, $P = 2.22E{-}28$, one-sided *t* test. **D,** Functional interaction map of the genes in Supplementary Table S2 generated using GeneMania (19). Nodes represent proteins. Edges indicate physical (red), pathway (blue), or shared domain (yellow) interactions. Nodes are grouped based on functional similarity. Edge thickness indicates number of studies in the literature supporting the interaction.

cellular functions (Fig. 1A). To identify common basal-A TNBC dependencies, a directed siRNA screen was performed on 4 other human basal-A cell lines and 3 luminal cell lines as controls using a customized 252 siRNA library (siGenome, Dharmacon) that targeted each of the 154 BPLER dependency genes (Fig. 1A). Transfection of each of these siRNAs individually reduced BPLER viability, suggesting that this library is enriched for functional siRNAs. To focus on genes that are not essential for viability of more differentiated cells, we excluded from consideration genes whose knockdown was lethal for the luminal cell lines. All seven cell lines used in the screen were efficiently transfected (>90%) and gave reproducible results under high-throughput screening conditions (Z' factor > 0.6). For each network, we assessed between 3 and 25 distinct siRNAs. The readout was the ratio in cell viability (*R*) between cells transfected with individual siRNAs versus nontargeting control, 72 hours after transfection. siRNAs returning an *R* value < 0.75 were considered hits. Each basal-A cell line displayed a unique vulnerability profile, not surprisingly given the genetic and epigenetic heterogeneity of these tumors (Fig. 1B; Supplementary Table S1). MB468 had the highest number of hits with 132 of 154 genes (213 of 252 siRNAs) scoring positive; HCC1954, HCC1937, and HCC1187 had 102, 91, and

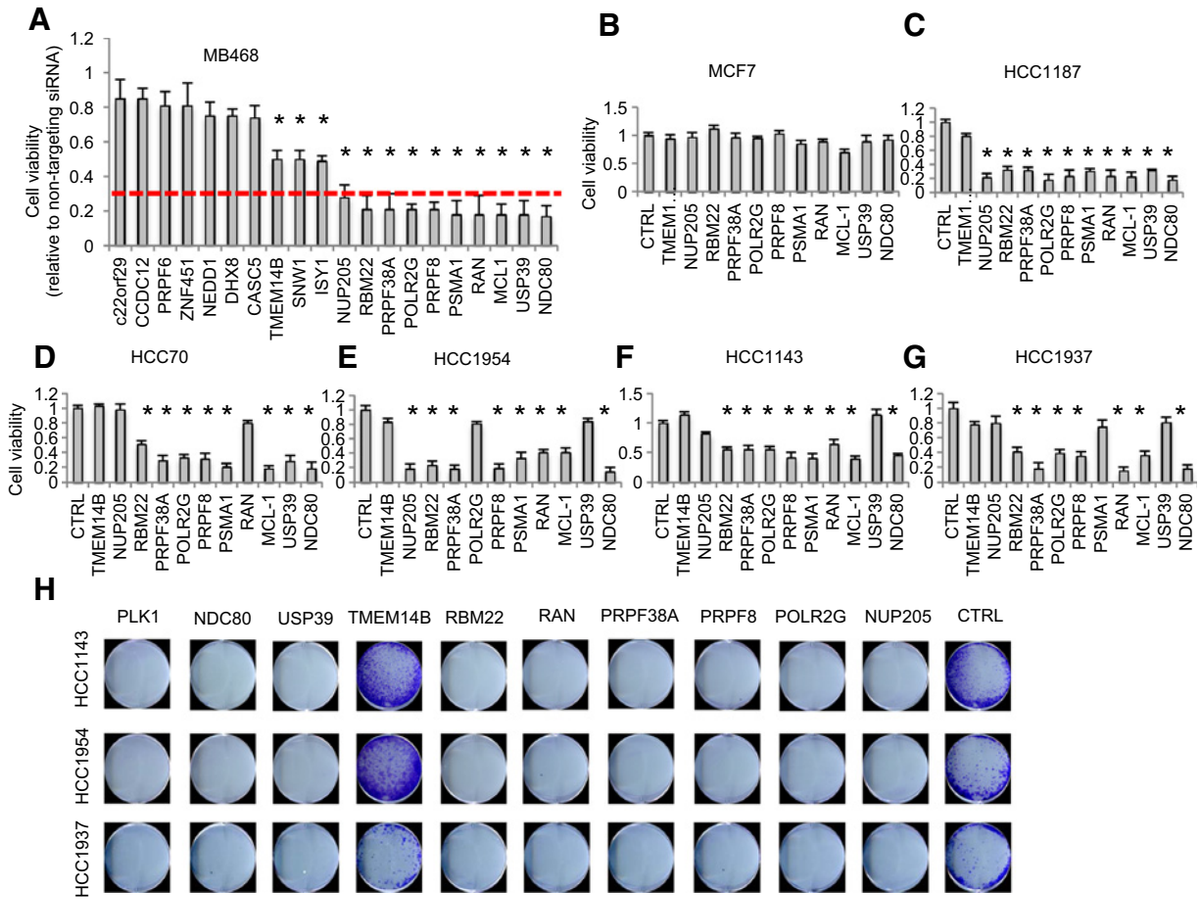

Figure 2.

Experimental validation using independent siRNAs of the top secondary screen hits involved in proteasome degradation, RNA splicing, mitosis, and nuclear transport. **A,** Viability of MB468 cells 72 hours after transfection with Silencer siRNAs targeting the indicated genes, relative to cells transfected with the nontargeting siRNA. Red line indicates the cutoff used for prioritizing genes for further validation (<0.3). **B–G,** Viability of MCF7 (**B**), HCC1187 (**C**), HCC70 (**D**), HCC1954 (**E**), HCC1143 (**F**), or HCC1937 (**G**) cells after transfection with Silencer siRNAs against the indicated genes or with a nontargeting siRNA (CTRL). All cell lines were assessed at 72 hours after transfection except for HCC1187 that were assessed at 96 hours. **H,** Colony assay of indicated cell lines after transfection with Silencer siRNAs against the indicated genes or nontargeting siRNA (CTRL). Cells were plated at clonal density 48 hours after transfection and grown for an additional 10 to 14 days. Colonies were visualized by crystal violet staining. PLK1 is shown as positive control. Data in **A** to **G** represent the mean ± SD of at least three independent experiments. *, $P < 0.05$ (one-sided t test).

44 gene hits (or 167, 122, and 65 siRNAs), respectively. Thirty genes scored with a ≥2-fold reduction in basal-A median cell viability. These were selected as high-confidence hits for further analysis (Supplementary Table S2). Similar results were obtained based on mean cell viability. The screen was not powered to systematically identify differential vulnerabilities between basal-A and luminal cell lines. Nonetheless, basal-A cell lines were generally more sensitive to knockdown of these genes than luminal cell lines (median $R = 0.39$ vs. 0.86; $P = 2.22\text{E}{-28}$, one-sided t test; Fig. 1C). RNA splicing (12 genes or 25 siRNAs; $q = 1.6\text{E}{-07}$) and ubiquitin-proteasome (5 genes or 9 siRNAs; $q = 0.007$) Reactome modules were overrepresented among these hits. The list also included the Bcl2-family gene *MCL1*, the mitotic spindle checkpoint genes *NDC80* and *CASC5*, and the nuclear transport genes *RAN* (also involved in mitosis) and *NUP205*. We previously showed that survival of basal-A cell lines depends on *MCL1* and the proteasome (9). TNBCs are well known to depend on mitosis. Both proteasome and RNA splicing hits formed a dense protein–protein interaction network based on GeneMania (ref. 19; Fig. 1D). NDC80 and CASC5 proteins were also predicted to interact. Thus, our siRNA screen reidentified known basal-like TNBC vulnerabilities and pointed to novel candidate targets, including specific RNA splicing and nuclear export genes.

Basal-A cell lines selectively depend on specific RNA splicing, mitosis, and nuclear export genes

To confirm the results of the screen, we selected 20 of the 30 high-confidence shared dependency genes for further experimental validation in MB468 cells (which scored positive for each of these hits in the primary screen) using a different siRNA (Silencer; Ambion; Fig. 2A), focusing on the most enriched functional pathways. Thirteen hits (65%) reconfirmed as MB468 dependency genes, based on the criteria used for the primary screen. Ten hits, whose knockdown reduced MB468 viability ≥3-fold, were

examined in 5 basal-A and 1 luminal cell line. These hits included genes involved in proteasome degradation (*PSMA1*), splicing (*PRPF8*, *PRPF38A*, *RBM22*, *POLR2G*, *USP39*), mitosis (*NDC80*), nuclear transport (*RAN*, *NUP205*), and apoptosis (*MCL1*). Knockdown of these genes had no significant effect on luminal MCF7 cell viability (Fig. 2B), but silencing *PSMA1*, *PRPF8*, *PRPF38A*, or *NDC80* (but not the nonvalidated hit *TMEM14B* used as control) reduced cell viability 72 to 96 hours after transfection by ≥3-fold in 4 of 5 basal-A cell lines (Fig. 2C–G). To further gauge the usefulness of these hits as candidate TNBC targets, we assessed the effect of gene knockdown on colony formation in 3 basal-A cell lines (HCC1143, HCC1954, and HCC1937; Fig. 2H). Knockdown of all 8 selected hits (but not *TMEM14B*) abrogated colony formation after 10 to 14 days, including hits that only weakly inhibited the short-term viability of these cell lines in bulk (e.g., *NUP205*, *USP39*).

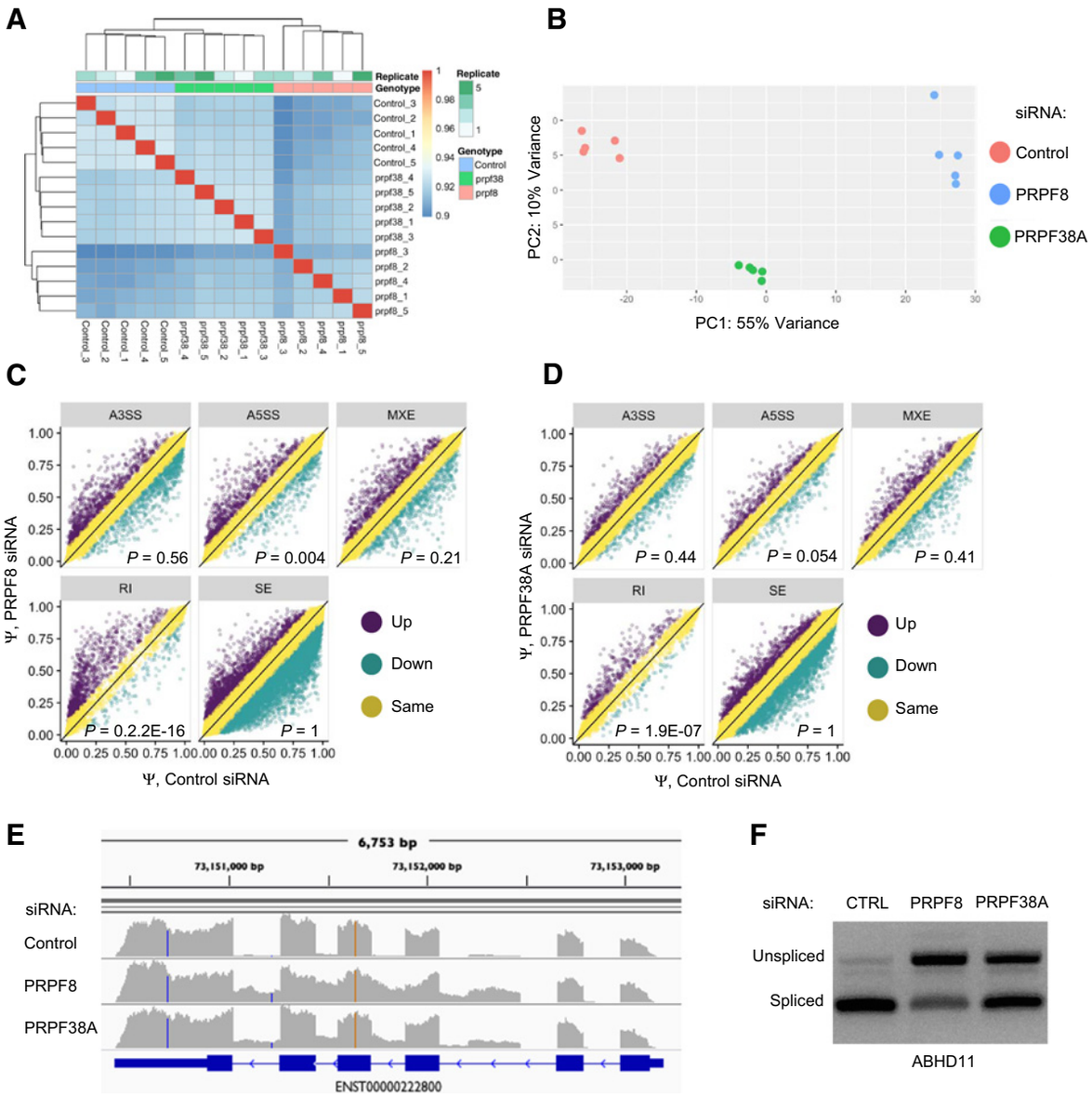

Figure 3.

PRPF8 or *PRPF38A* knockdown triggers intronic retention. **A,** Correlation (Spearman) of gene expression of TMM-normalized RNA-seq counts from five independent replicates of viable control (transfected with nontargeting siRNA), PRPF8-KD, PRPF38A-KD MB468 cells. Heatmap shows clustering of replicate samples. **B,** PCA of RNA-seq gene-level expression data in the same samples as in **A**, using the 500 most variable genes. **C** and **D,** MISO analysis of specific classes of RNA splicing alterations within differentially expressed transcripts in PRPF8-KD (**C**) and PRPF38A-KD (**D**) samples relative to control samples transfected with nontargeting siRNA. $P<0.05$ indicates significant enrichment for alterations of the indicated class (Wilcoxon test). **E,** RNA-seq read coverage for *ABHD11* in PRPF8-KD and PRPR38A-KD and control cells. Blue boxes and lines indicate exonic and intronic regions, respectively. **F,** RT-PCR, using intron-spanning primers for *ABHD11*, of total RNA from MB468 cells 48 hours after transfection with the indicated siRNAs. Intron-retaining transcripts migrate more slowly.

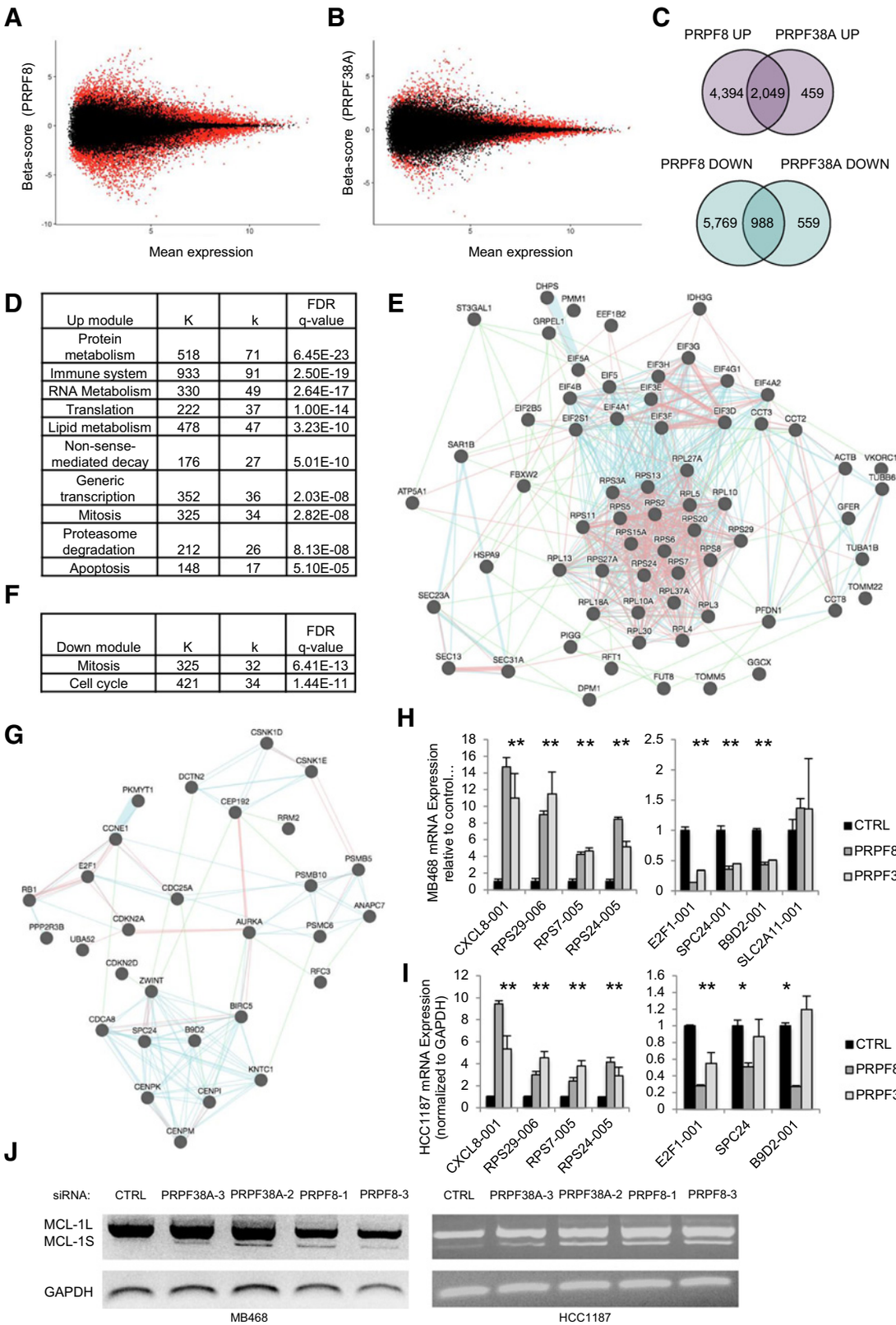

Up module	K	k	FDR q-value
Protein metabolism	518	71	6.45E-23
Immune system	933	91	2.50E-19
RNA Metabolism	330	49	2.64E-17
Translation	222	37	1.00E-14
Lipid metabolism	478	47	3.23E-10
Non-sense-mediated decay	176	27	5.01E-10
Generic transcription	352	36	2.03E-08
Mitosis	325	34	2.82E-08
Proteasome degradation	212	26	8.13E-08
Apoptosis	148	17	5.10E-05

Down module	K	k	FDR q-value
Mitosis	325	32	6.41E-13
Cell cycle	421	34	1.44E-11

RNA splicing genes are commonly upregulated in basal-like primary tumors

Many of the shared basal-A dependency genes are involved in splicing. To explore splicing as a potential TNBC drug target, we examined expression of 72 genes associated with different steps of RNA splicing (based on the MSigDB database) in 476 human breast specimens in the TCGA database, including 387 primary tumors (109 basal-like, 268 luminal) and 99 normal breast tissues. Hierarchical clustering based on these genes separated basal-like and luminal tumors and normal breast tissue. Basal-like tumors showed the highest spliceosome gene expression (Supplementary Fig. S1A). Splicing genes, as a group, were modestly, but significantly, upregulated in basal-like tumors relative to luminal tumors and normal breast (mean fold change: 1.2 and 1.4, respectively; $P = 0.007$ and 1.8E−9 by two-sided t test; Supplementary Fig. S1B). Ten genes were upregulated by ≥2-fold *SF3B4* (in the SF3b complex), *LSM2*, *LSM4*, and *LSM7* (in the tri-snRNP complex), and Sm proteins associated with snRNP biogenesis (*SNRPA*, *SNRPB*, *SNRPC*, *SNRPD1*, *SNRPE*, *SNRPG*; Supplementary Fig. S1C). None of the RNA splicing dependency gene mRNAs in our screen were upregulated by ≥1.5-fold in basal-like TNBCs compared with luminal or normal tissues and thus would have been difficult to identify by mRNA expression. However, PRPF8, PRPF38A, and RBM22 proteins were generally more abundant in luminal and TNBC (both basal-A and basal-B) cell line lysates than in BPE, a nontransformed breast epithelial cell line (Supplementary Fig. S1D). Moreover, knockdown of each of these three genes selectively triggered caspase-3 cleavage in MB468, but not BPE, confirming the functional relevance of these hits (Supplementary Fig. S1E).

PRPF8 and *PRPF38A* are both required for optimal RNA splicing

PRPF8 is a core component of the *Saccharomyces cerevisiae* and human U4/U6.U5 tri-snRNP complexes (15–17). Prp38, the yeast homolog of PRPF38A, is required for catalytic activation of the tri-snRNP complex (24, 25). Thus, PRPF8 and PRPF38A are both important for the tri-snRNP function. To study early events associated with inhibiting this complex, we first validated 2 sets of siGenome siRNAs (4 individual siRNAs each) against *PRPF8* (PRPF8-01, -02, -04, -05) and *PRPF38A* (PRPF38A-01, 02, 03, 04). All 8 siRNAs induced >90% target mRNA silencing in MB468 cells 48 hours after transfection as determined by qRT-PCR (Supplementary Fig. S2A). PRPF8 and PRPF38A protein knockdown was confirmed by immunoblot for 2 of 2 PRPF8 (PRPF8-01, -02) and 2 of 2 PRPF38A siRNAs (PRPF38A-02, -03) tested (Supplementary Fig. S2B). Unlike *PRPF38A* Silencer siRNA (Supplementary Fig. S1E), neither PRPF38A-02 nor PRPF38A-03 siGenome siRNAs suppressed PRPF8 proteins levels.

Next, we performed RNA-seq in quintuplicate in MB468 cells knocked down for *PRPF8* (PRPF8-KD) or *PRPF38A* (PRPF38A-KD) for 48 hours using PRPF8-01 and PRPF38A-03 siRNAs, respectively. Note that 50% to 70% of cells were viable, and only live cells were analyzed. The dominant *PRPF8* isoform was knocked down by >98%, although a minor isoform, comprising approximately 5% of *PRPF8* transcripts, persisted based on the estimated TPM values from Sailfish (26). All 3 known splicing variants of *PRPF38A* were silenced by >95%. Replicate samples clustered based on Spearman correlation of TMM-normalized counts (Fig. 3A). Principal component analysis (PCA) on the 500 most variable genes clearly separated PRPF8A-KD, PRPF38A-KD, and control samples (Fig. 3B; QC data available on line).

To determine how PRPF8 or PRPF38A affect RNA splicing, we first assessed the relative representation of specific classes of splicing events in PRPF8-KD and PRPF38A-KD, alternative 5′ splice sites (A5SS), alternative 3′ splice sites (A3SS), mutually exclusive exons (MXE), retained introns (RI), and skipped exons (SE), based on MISO analysis (ref. 27; Fig. 3C and D). Both PRPF8-KD and PRPF38A-KD had significantly higher RIs than control cells ($P = 2.2E{-}16$ and $P = 1.9E{-}07$, respectively; Wilcoxon test). PRPF8-KD also showed greater A5SS ($P = 0.004$) use, but this association was weaker in PRPF38A-KD ($P = 0.054$). There were no significant differences in A3SS, MXE, or SE with knockdown of either gene. Among 5,231 introns considered in MISO, 1,261 (24.1%) and 535 (10.2%) showed ≥10% differential retention in PRPF8-KD and PRPF38A-KD, respectively (Supplementary Table S3). Of note, 83% of retained introns in PRPF38A-KD were also found in PRPF8-KD, suggesting that the two proteins affected RNA splicing through a similar mechanism. RT-PCR verified that both *PRPF8* and *PRPF38A* knockdown caused intronic retention in *ABHD11* transcripts, randomly chosen among the top shared differential RI events (Fig. 3E and F). Thus, both *PRPF8* and *PRPF38A* were required for optimal RNA splicing, although *PRPF8* more than *PRPF38A*.

PRPF8 recapitulates the functional effect of *PRPF38A* on gene expression

We next used DESeq2 software (28) to examine whether *PRPF8* and *PRPF38A* silencing selectively affects the expression of certain types of genes (Supplementary Tables S4 and S5). Note that 1,293 and 2,261 mRNAs were up- and downregulated by ≥2-fold, respectively, in PRPF8-KD relative to control cells with q value < 0.01 (excluding genes with <20 normalized counts).

Figure 4.

PRPF8 or *PRPF38A* knockdown regulates splice variants of genes implicated in protein metabolism, mitosis, proteasome function, and apoptosis. **A** and **B,** Bland–Altman (MA) plots of transcript-level mean expression by RNA-seq in viable MB468 cells 48 hours after transfection with *PRPF8* (**A**) or *PRPF38A* (**B**) siRNAs, relative to nontargeting siRNA. B score is the beta coefficient from the Sleuth analysis. Red indicates $q < 0.05$. **C,** Venn diagrams showing the number of shared upregulated (top) or downregulated (bottom) transcripts in MB468 cells transfected with *PRPF8* or *PRPF38A* siRNAs relative to nontargeting siRNA. **D,** Significantly overrepresented Reactome modules ($q < 0.01$) among upregulated transcripts in PRPF8-KD and PRPF38A-KD cells. Full list in Supplementary Table S8. *K* indicates the total number of genes in each module; *k* indicates the number of upregulated transcripts assigned to each module. **E,** Functional interaction map of protein metabolism proteins corresponding to transcripts upregulated in viable PRPF8-KD and PRPF38A-KD. Map generation and interaction key as in Fig. 1D. **F,** Significantly overrepresented Reactome modules ($q < 0.01$) among downregulated transcripts in MB468 cells knocked down for *PRPF38A*, as in **D**. Full list in Supplementary Table S9. **G,** Functional interaction map of mitosis proteins (based on MSigDB) corresponding to transcripts downregulated in viable PRPF8-KD and PRPF38A-KD cells as in **E**. **H** and **I,** Levels of the indicated transcripts in MB468 (**H**) or HCC1187 (**I**) 48 hours after transfection with siRNAs against *PRPF8* or *PRPF38A* relative to nontargeting siRNA, as determined by qRT-PCR using isoform-specific primers. Data represent the mean ± SD of at least two independent experiments (*, $P < 0.05$; t test relative to control). **J,** RT-PCR analysis of *MCL1* splicing using primers that distinguish between different *MCL1* isoforms in MB468 and HCC1187 cells 48 hours after transfection with indicated siRNAs. Top and bottom bands correspond to *MCL1-001* and *MCL1-002* transcripts, respectively.

PRPF38A-KD showed a more restricted effect with 579 up- and 610 downregulated genes based on the same criteria (Supplementary Fig. S2C and S2D). Among the genes up- and downregulated in PRPF38A-KD, 70% and 75% were similarly changed in PRPF8-KD (Supplementary Fig. S2E). To estimate the reproducibility of the RNA-seq data, we selected a set of 12 genes and measured their expression by qRT-PCR. Ten of 12 genes reconfirmed as differentially expressed in PRPF8-KD, and all 12 genes reconfirmed as differentially expressed in PRPF38A-KD cells, with fold changes between 2 and 33. Eighty percent of the expressed genes, validated as differentially expressed in PRPF8-KD or PRPF38A-KD, showed similar changes in HCC1187 knocked down for *PRPF8* or *PRPF38A* (Supplementary Fig. S2G). Thus, much of the effect of PRPF38A on gene expression was recapitulated by PRPF8, but not vice versa.

PRPF8 and *PRPF38A* knockdown affects the pre-mRNA splicing of well-defined classes of genes required for TNBC survival

We next used Sleuth software to evaluate the expression of specific splice variants in PRPF8-KD and PRPF38A-KD. Of 196,501 transcripts, 29,980 (15.2%) and 16,955 (8.6%) transcripts were differentially expressed in PRPF8-KD and PRPF38A-KD, respectively (Fig. 4A and B; Supplementary Tables S6 and S7). We further analyzed transcripts with a β-score ≥ 0.69 or ≤ -0.69 (approximately 3-fold change) and $q \leq 0.01$. Based on these criteria, 6,443 transcripts were upregulated and 6,767 were downregulated in PRPF8-KD cells, whereas 2,508 were upregulated and 1,557 were downregulated in PRPF38A-KD cells (Fig. 4C). Eighty-two percent and 64% of up- and downregulated transcripts in PRPF38A-KD cells were similarly altered in PRPF8-KD cells, corroborating the link between PRPF8 and PRPF38A.

Reactome pathway analysis (29) of shared *PRPF8*- and *PRPF38A*-dependent transcripts identified at least 100 overrepresented modules ($q < 0.01$; Fig. 4D and Supplementary Table S8). Upregulated transcripts were particularly enriched for immune system protein genes (e.g., *CXCL8*, *IL6*, *TNF*), ribosomal protein genes (e.g., *RPS5*, *RPS6*, *RPS24*), and translation initiation factors (e.g., *EIF4A1*, *EIF4A2*, *EIF4G1*). Genes involved in mitosis (e.g., *AURKB*, *CENPA*, *CENPN*), the proteasome (e.g., *PSMA3*, *PSMB4*, *PSMD2*), and apoptosis (e.g., *MCL1*, *TP53*, *DIABLO*, *BAX*, *CASP7*, *TNF*) were also highly enriched (Fig. 4E). These transcripts were frequently RI or nonsense variants encoding for nonfunctional proteins. Specifically, 41 of 56 (73%) of translation initiation, 63 of 98 (64%) of protein metabolism (mainly ribosomal protein transcripts), 18 of 38 (47%) of mitosis, and 16 of 34 (47%) of proteasome-related transcripts were inactive splice variants. In contrast, key immune system transcripts were protein-coding variants. Therefore, both *PRPF8* and *PRPF38A* knockdown altered the pre-mRNA splicing of well-defined classes of genes, some of which directly control apoptosis or are known to be selectively required for TNBC survival (e.g., mitosis and proteasome genes). Conversely, downregulated transcripts in PRPF8-KD and PRPF38A-KD were mostly enriched for genes implicated in mitosis and the mitotic spindle checkpoint (Fig. 4F and G; Supplementary Table S9). Unlike the upregulated mitosis transcripts, 30 of 35 (86%) of downregulated mitosis transcripts were protein-coding variants. These data were validated by flow cytometry and immunoblot experiments, which showed that *PRPF8* knockdown increased by 45% the number of cells in G_2–M phase (from 29% to 42%; Supplementary Fig. S3A) and increased phosphorylated histone H3 protein levels (Supplementary Fig. S3B), confirming that mitosis was disrupted.

To further corroborate these data, we measured the expression of eight deregulated transcripts (four up and four down) that could be unequivocally distinguished by qRT-PCR using isoform-specific primers, focusing on immune (up), ribosomal (up), and mitosis (down)-related transcripts (Fig. 4H). Seven of 8 transcripts were differentially expressed by approximately 2- to 12-fold in both PRPF8-KD and PRPF38A-KD. Of these, 7 and 5 were also differentially expressed by >2-fold in HCC1187 cells knocked down for *PRPF8* or *PRPF38A*, respectively (Fig. 4I).

We next asked whether any of the top basal-A dependency genes (Supplementary Table S2) were affected by *PRPF8* and *PRPF38A* knockdown. *MCL1* (ranked #2 in our screen), *PSMB4*, *POLR2G*, *C22orf29*, *ZNF451*, *ZNF552*, and *ZNF585A* each had at least one transcript with β-score ≤ -0.69 or ≥ 0.69 and $q \leq 0.01$ in both PRPF8-KD and PRPF38A-KD. In particular, the MCL1-002 transcript that encodes for the proapoptotic protein Mcl-1_S was upregulated in both PRPF8-KD and PRPF38A-KD, whereas the MCL1-001 transcript that encodes for antiapoptotic Mcl-1_L was downregulated in PRPF8-KD. These results were confirmed by RT-PCR using 2 different siRNAs for PRPF8 and PRPF38A (Fig. 4J, left). In HCC1187 cells, both Mcl-1_S and Mcl-1_L transcripts were induced by knockdown of *PRPF8* or *PRPF38A* (Fig. 4J, right). Thus, *PRPF8* and *PRPF38A* knockdown enhanced expression of proapoptotic Mcl-1_S.

To exclude potential off-target effects, we selected a subset of transcripts implicated in immune response (CXCL8-001), protein translation (RPS29-006, RPS7-005, RPS24-005), cell cycle (E2F1-001), mitosis (SPC4-001, B9D2-001), the proteasome (PSMB10-003), and apoptosis (MCL1-002) and reassessed each of them separately in nontransformed BPE cells and five breast cancer cell lines of different subtypes, using two to four prevalidated *PRPF8* siRNAs (Supplementary Figs. S4 and S5). Changes in splicing of all these transcripts, except *CXCL8* and *PSMB10*, were found using at least two distinct siRNAs in three or more cell lines (Supplementary Table S10). Taken together, these data indicate that certain classes of transcripts, including multiple TNBC dependency genes, are altered by *PRPF8* or *PRPF38A* knockdown.

The splicing modulator E7107 affects multiple TNBC survival networks and is cytotoxic against basal-A cells

E7107 is a clinical-stage small molecule that perturbs the activity of the core splicing factor SF3B1. Its effect on *PRPF8* or *PRPF38A* function is unknown. Because SF3B1 is essential for splicing and operates upstream of the tri-snRNP complex, we postulated that E7107 may affect *PRPF8*- and *PRPF38A*-sensitive transcripts and thus basal-like TNBC survival networks. To explore this hypothesis, we assessed genome-wide mRNA expression changes associated with exposure to E7107 for 24 hours using MB468 as a model. A total of 11,217 and 15,869 transcripts were upregulated and downregulated, respectively, based on the same sleuth criteria used for *PRPF8* and *PRPF38A* RNA-seq analysis (Supplementary Table S11). The majority of upregulated transcripts (58%) were noncoding variants (mostly intron-retaining), similar to what observed after *PRPF8* or *PRPF38A* knockdown. To define functional pathways most affected by E7107, we focused on the top 1,000 up- and downregulated transcripts based on *b*-value. Both genesets were enriched for genes involved in mitosis, RNA splicing, DNA repair, proteasome degradation, and nuclear transport ($q < 0.01$ for each module; Supplementary Tables S12

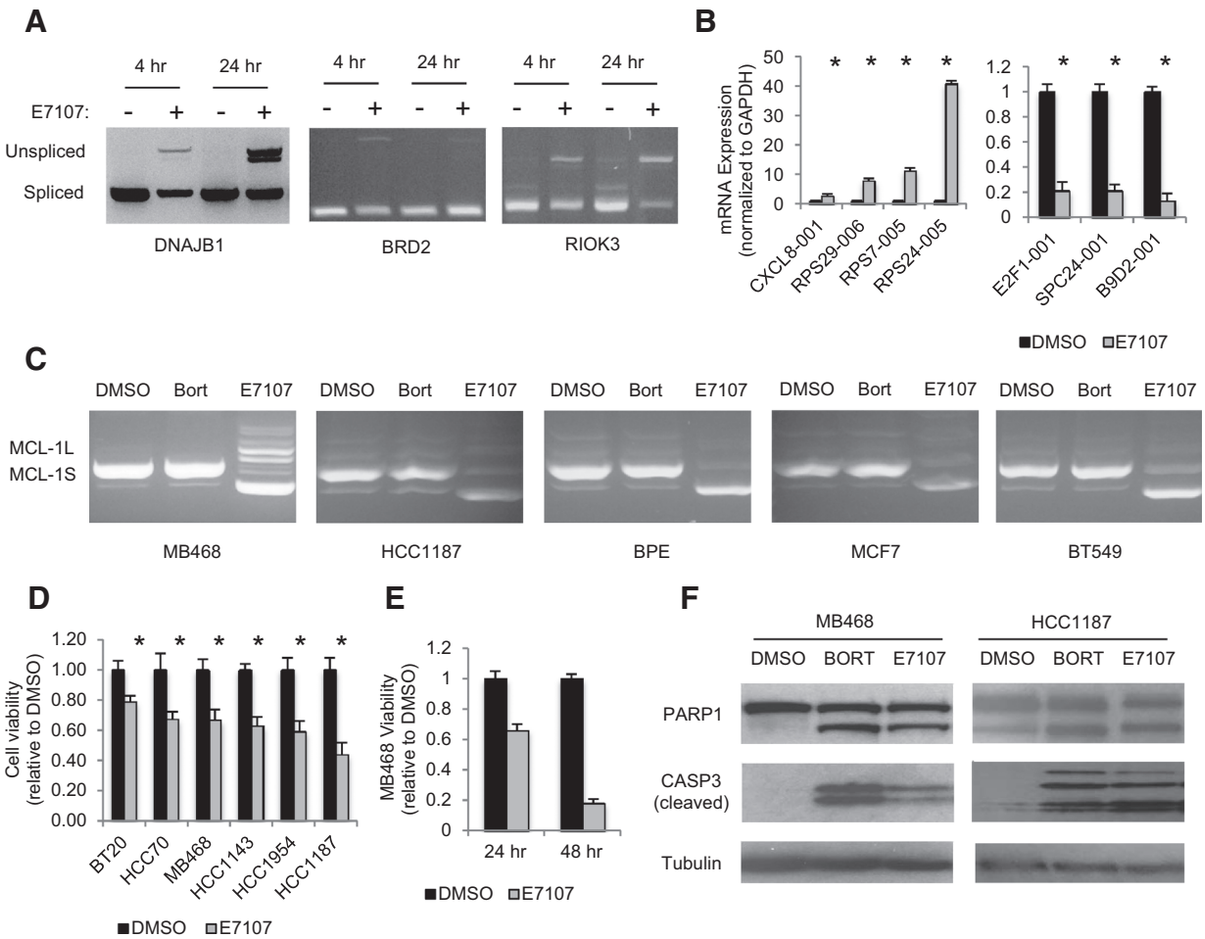

Figure 5.

The splicing modulator drug E7107 causes intron retention, affects *PRPF8*- and *PRPF38A*-sensitive splice variants, and promotes apoptosis in basal-A cell lines *in vitro*. **A,** RT-PCR using intron-spanning primers for the indicated genes of total RNA from MB468 cells treated with 100 nmol/L E7107 (+) or DMSO (−) for the indicated time. **B,** Transcript mRNA levels, determined by qRT-PCR of the indicated genes using isoform-specific primers, in MB468 cells treated with 100 nmol/L E7107 or DMSO for 24 hours. Data represent the mean ± SD of at least three independent experiments (*, $P < 0.05$; *t* test relative to control). **C,** RT-PCR analysis of *MCL1* splicing as in Fig. 4J in the indicated cell lines treated with E7107, bortezomib (Bort; used as control), or DMSO for 24 hours. **D** and **E,** Viability of indicated cell lines after treatment with E7107 or DMSO after 24 hours (**D**) or after culture for an additional 24 hours in drug-free medium (**E**), relative to DMSO-treated cells. Data represent the mean ± SD of at least three independent experiments (*, $P < 0.05$; *t* test relative to control). **F,** Immunoblot probed for the indicated proteins of lysates of MB468 and HCC1187 cells treated with 100 nmol/L E7107, 12.5 nmol/L Bortezomib (Bort), or DMSO for 24 hours.

and S13). Among PRPF8/PRPF38A-sensitive mRNAs, 42.5% of upregulated and 28.2% of downregulated transcripts were similarly affected by E7107 in the same direction, which is more than expected by chance ($P = 9.6E{-}68$ and $P = 0.04$, respectively, by hypergeometric distribution).

To begin to validate these data, we assessed by qRT-PCR or RT-PCR the expression of 11 of these transcripts in MB468 cells 24 hours after treatment with E7107. E7107 caused marked intronic retention based on the accumulation of unspliced transcripts of *DNAJB1*, *BRD2*, and *RIOK3* (Fig. 5A). Like *PRPF8* and *PRPF38A* knockdown (Fig. 4H and I), E7107 activated the protein-coding isoform of *CXCL8*, induced intron-retaining transcripts of ribosomal proteins *RPS7*, *RPS24*, and *RPS29*, and suppressed protein-coding variants of *E2F1* and spindle checkpoint *SPC24* and *B9D2* transcripts (Fig. 5B). Moreover, E7107 altered *MCL1* splicing to the proapoptotic splice variant in 5 breast cell lines, including nontransformed BPE cells (Fig. 5C). The effect of E7107 on *MCL1* splicing was not secondary to cell death, because *MCL1* splicing was not affected by bortezomib, which is cytotoxic to basal-A TNBC cell lines (ref. 9; Fig. 5C). Thus, E7107 recapitulated key splicing effects of *PRPF8* and *PRPF38A* knockdown and affected similar processes implicated in basal-like TNBC survival.

We next tested whether E7107 treatment was cytotoxic against basal-like TNBC cells *in vitro*. Among 6 basal-A lines tested, 5 showed <66% viability 24 hours after treatment compared with vehicle-treated cells (Fig. 5D). In MB468, viability declined to <20% after an additional 24 hours in drug-free medium, suggesting that the cells had become committed to death (Fig. 5E). The sensitivity of other cell lines at 48 hours was not tested. In both HCC1187 and MB468, E7107 activated PARP1 and caspase-3

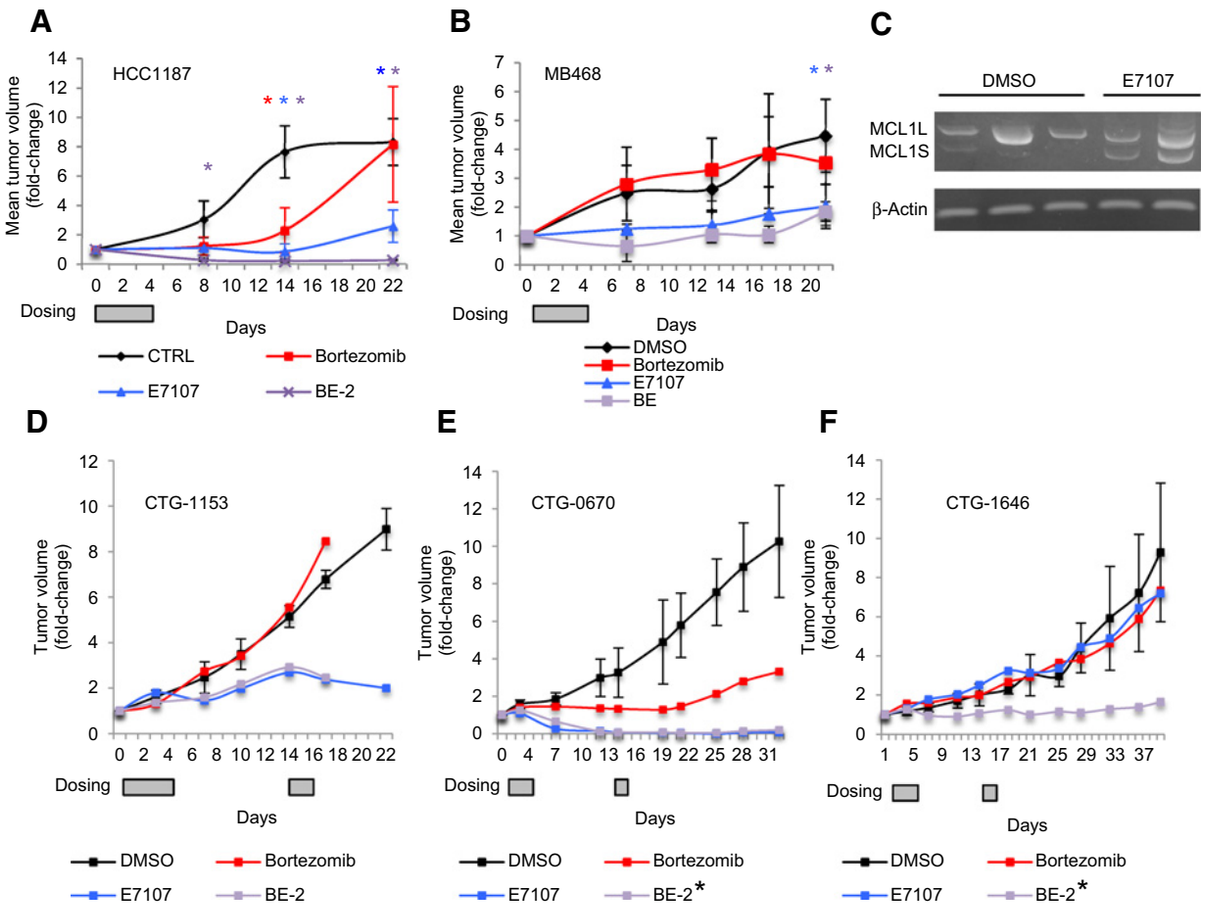

Figure 6.

E7107 impedes *in vivo* growth of cell line– and patient-derived TNBC xenografts, and its activity is augmented in combination with bortezomib. **A** and **B,** Mean tumor volume fold change (relative to day 0) ± SD in mice bearing palpable HCC1187 ($n = 16$; **A**) or MB468 ($n = 16$; **B**) xenografts in the right flank treated with intravenous bortezomib (0.4 mg/kg; red), E7107 (5 mg/kg; blue), both (purple), or DMSO (black) on days 1 to 4, according to the BE-2 dosing schedule, as shown in Supplementary Table S14. *, significant difference ($P < 0.05$; one-sided *t* test) for bortezomib (red), E7107 (blue), or both (purple) relative to DMSO. **C,** RT-PCR analysis of *MCL1* splicing as in Fig. 4J in preestablished MB468 xenografts 6 hours after treatment with one E7107 dose (5 mg/kg) or DMSO. **D** and **E,** Tumor volume in mice bearing palpable CTG1153 ($n = 4$; **D**), CTG0670 ($n = 4$; **E**), or CTG1646 ($n = 4$; **F**) TNBC PDXs in the right flank treated with bortezomib (0.4 mg/kg; red), E7107 (5 mg/kg; blue), both (purple), or DMSO (black) on days 1 to 4, 15, and 16, according to the BE-2 (CTG1153) or BE-2* (CTG0670 and CTG1646) dosing schedules, as shown in Supplementary Table S14. Data represent individual tumor volumes (relative to pretreatment volume) for each mouse. Gray boxes in **A**, **B**, and **D–F** indicate treatment days.

cleavage, two indicators of apoptosis, within 24 hours (Fig. 5F). *SF3B1* knockdown also killed both cell lines (Supplementary Fig. S6). These data suggest that *SF3B1* modulators might be harnessed therapeutically to target multiple basal-like TNBC dependencies at once.

E7107 impedes TNBC growth in both cell line and PDX models

We next evaluated E7107 in 5 mouse TNBC models—2 basal-A cell line xenografts (HCC1187 and MB468 in Nu/J mice) and 3 basal-like TNBC PDXs (CTG0670, CTG1153, and CTG1646 in NCr mice). E7107 (5 mg/kg) was administered when tumor volume reached approximately 100 mm^3 (day 0) by tail-vein injection for 4 days (1–4) or 4 + 2 days (1–4, 15, 16) in the cell line and PDX models, respectively. In the HCC1187 model, E7107 decreased mean primary tumor volume by 80% after 22 days, compared with vehicle ($P = 0.002$, one-sided *t* test; Fig. 6A). Comparable results were obtained in a replicate experiment (Supplementary Fig. S7A). MB468 xenografts were also sensitive to E7107 (55% mean tumor volume reduction after 21 days; $P = 0.01$, one-sided *t* test; Fig. 6B). Within MB468 xenografts, E7107 induced $MCL1_S$ expression as early as 6 hours after a single dose, although $MCL1_L$ expression persisted (Fig. 6C).

The PDX models originate from heavily pretreated basal-like TNBC patients, who were refractory to an anthracycline, cyclophosphamide, and paclitaxel. To assess the therapeutic effect of E7107, we adopted a "one animal per model per treatment" ($1 \times 1 \times 1$) study design (30), but included 3 animals in the control group to estimate the variability of each model. For each PDX, all vehicle-treated animals developed tumors that expanded over 22 to 38 days (Fig. 6D–F). E7107 induced a partial response in CTG1153 (74% tumor volume reduction compared with control mean after 22 days; Fig. 6D) and complete response in

CTG0670 (>99% tumor volume reduction relative to control mean after 12 days; Fig. 6E), whereas it was ineffective against CTG1646 (Fig. 6F).

The combination of E7107 and bortezomib improves tumor response

We previously showed that bortezomib is effective against basal-A TNBC xenografts, but only at the MTD (9). To test whether bortezomib could augment E7107 antitumor activity, we first conducted a tolerability study in HCC1187 tumor–bearing Nu/J mice using increasing doses of bortezomib and a fixed E7107 dose (125 μg, ∼5 mg/kg), coadministered intravenously. We assessed 5 bortezomib/E7107 (BE) regimens (Supplementary Table S14). BE-3 was the MTD. BE-2 (50% the MTD), which was well tolerated, was used for all efficacy studies. This low dose of bortezomib (10 μg, ∼0.4 mg/kg) alone has no therapeutic effect in these models. As above, cell line xenografts were treated for 4 days (1–4) and PDXs for 4 + 2 days (1–4, 15, 16). BE-2 induced nearly complete response against preestablished HCC1187 xenografts after 8 days (92% mean tumor volume reduction; $P = 0.01$, one-sided t test; Fig. 6A), whereas neither bortezomib nor E7107 alone did. BE-2 somewhat improved the response to E7107 in MB468 xenografts but not significantly (Fig. 6B).

We next assessed the combination in PDX models. In CTG1153, BE-2 was lethal after 16 days, suggesting that BE-2 is less well tolerated in NCr than Nu/J mice. BE-2 did not improve the CTG1153 response to E7107 over this time (Fig. 6D). We next tested reducing the number of injections of bortezomib from 3 to 2 without changing E7017 dosing (BE-2*; Supplementary Table S14) in CTG1646 and CTG0670. BE-2* was well tolerated in both models for over 30 days. In CTG0670, E7107 with or without bortezomib induced a complete response (Fig. 6E). In CTG1646, where neither E7107 nor bortezomib had a significant effect on its own, the combination reduced tumor volume by 85% compared with control mice (Fig. 6F). Overall, a bortezomib/E7107 combination reduced tumor volume in five of five TNBC models, inducing a complete or nearly complete response in two models.

Discussion

Here, we used a previous siRNA genetic dependency screen in one basal-A TNBC cell line (BPLER) as a starting point to identify common gene dependencies of basal-like TNBC as potential drug targets. Only 30 of 154 BPLER dependency genes were shared with other basal-A TNBC cell lines, consistent with this subtype's heterogeneity. These 30 genes included 5 proteasome genes and *MCL1*, which we previously identified as shared dependencies of basal-A TNBC. Another prominent set of genes (12 of the remaining 24) function in RNA splicing. Although splicing involves hundreds of genes, these hits concentrated in a particular splicing complex, the U4/U6.U5 tri-snRNP complex, which joins the spliceosome complexes at the 5′ and 3′ ends of introns at an early step of intron excision. Indeed, TNBC cells knocked down for either of two tri-snRNP genes, *PRPF8* and *PRPF38A*, showed widespread intron retention. Splicing alterations were not randomly distributed, but were concentrated in mRNAs participating in vital processes on which TNBCs are known to depend, including protein translation (especially ribosomal proteins and translation initiation factors), protein degradation, mitosis, cell-cycle progression, and the immune response. Abnormal splicing of *MCL1* increased expression of its proapoptotic splicing variant and reduced expression of its antiapoptotic variant. Treatment with the SF3B1 modulator E7107 similarly affected *MCL1*, suggesting that *MCL1* splicing is sensitive to RNA splicing perturbation, confirming previous reports (31, 32), and not uniquely dependent on the tri-snRNP complex. E7107 also affected different gene networks critically implicated in TNBC survival, including mitosis, proteasome degradation, RNA splicing, nuclear export, and DNA repair. Thus, multiple mechanisms, beside *MCL1* inhibition, are likely involved in TNBC response to E7107. Additional studies will be needed to dissect the precise contribution of each of these mechanisms, particularly *in vivo*.

We first investigated the effect of knocking down tri-snRNP genes, which were high-confidence hits in our screen. No prior studies have looked at how these splicing factors affect pre-mRNA expression or splicing on a genome-wide scale. *PRPF8* acts as a scaffold to assemble the complex. The function of *PRPF38A* is less clear. *PRPF38A* interacts with 28 other RNA splicing proteins, including tri-snRNP proteins, A complex proteins, B complex proteins, proteins involved in B complex activation, and U2 snRNA-interacting proteins. As such, *PRPF38A* is one of the largest protein–protein interaction hubs of the human spliceosome (25).

RNA sequencing of cells knocked down for *PRPF8* or *PRPF38A* showed that certain groups of functionally related transcripts are selectively sensitive to tri-snRNP disruption. Ribosomal protein transcripts comprised the most overrepresented class of differentially spliced transcripts. This makes sense, because these mRNAs have short half-lives (∼8–15 minutes). Mitosis and apoptosis transcripts (also enriched) also have short half-lives (33). Together, these data suggest that transcripts that turnover rapidly may be most affected by a dysfunctional spliceosome. The fact that the same transcripts were similarly affected in 6 cell lines (including non-transformed cells) suggests that certain genes may be intrinsically susceptible to splicing inhibition. Another key finding is that new transcripts are frequently intron-retaining or nonsense splice variants. Knockdown of these splicing genes selectively affected genes/pathways that are specific dependencies of basal-A TNBC cells, including mitosis, the ubiquitin–proteasome system, and *MCL1*. Thus, suppressing splicing could be a way to target multiple TNBC vulnerabilities at once.

Splicing is emerging as an attractive therapeutic target for both hematologic and solid malignancies (34). Human cancers frequently co-opt the RNA splicing machinery to reprogram gene expression to their advantage. Although several splicing modulator natural products have been identified, only one splicing modulator drug, E7107, a derivative of pladienolide D, which perturbs SF3B1 activity (12, 18, 35), has been tested in the clinic (36, 37). A second-generation modulator of the SF3b complex, dubbed H3B-8800, is currently in phase I trials, but no data have been released yet. To our knowledge, no selective modulators of the tri-snRNP complex are currently available for clinical testing. Although our study suggests that key TNBC survival networks are equally sensitive to inhibition of the SF3b and tri-snRNP complexes *in vitro*, it will be interesting to define whether specific modulation of either complex is associated with distinct safety and efficacy profiles *in vivo*. Here, we showed, for the first time, that E7107 monotherapy induced a complete response in a TNBC PDX model. Our data also suggest that combining splicing modulation with proteasome inhibition should enhance antitumor efficacy and broaden responses.

Disclosure of Potential Conflicts of Interest

No potential conflicts of interest were disclosed.

Disclaimer

The content is solely the responsibility of the authors and does not necessarily represent the official views of the NIH.

Authors' Contributions

Conception and design: S. Chan, P. Sridhar, J. Lieberman, F. Petrocca
Development of methodology: S. Chan, P. Sridhar, Z. Herbert, F. Petrocca
Acquisition of data (provided animals, acquired and managed patients, provided facilities, etc.): S. Chan, P. Sridhar, Y.J. Lock, Z. Herbert, F. Petrocca
Analysis and interpretation of data (e.g., statistical analysis, biostatistics, computational analysis): S. Chan, P. Sridhar, R. Kirchner, P. Smith, J. Lieberman, F. Petrocca
Writing, review, and/or revision of the manuscript: S. Chan, P. Sridhar, S. Buonamici, P. Smith, J. Lieberman, F. Petrocca
Administrative, technical, or material support (i.e., reporting or organizing data, constructing databases): P. Sridhar
Study supervision: J. Lieberman, F. Petrocca

Acknowledgments

We thank Tony Godfrey of Boston University for useful discussions, Arya Ashok and Maria Mancini of Champions Oncology for PDX-related studies; Caroline Shamu, Jennifer Smith, and Sean Johnston of ICCB-L Screening Facility for help with siRNA screening; and all members of the Lieberman and Petrocca laboratories for helpful suggestions.

Research reported in this publication was supported by the NCI of the NIH under award number 5K22CA184244 (to F. Petrocca), by a Boston University/Boston Medical Center Startup Fund (to F. Petrocca), and by a Breast Cancer Alliance Exceptional Project Grant (to J. Lieberman). Approximately 50% of the project costs were financed by federal money and the remaining 50% by nongovernmental sources.

The costs of publication of this article were defrayed in part by the payment of page charges. This article must therefore be hereby marked *advertisement* in accordance with 18 U.S.C. Section 1734 solely to indicate this fact.

Received May 21, 2017; revised August 21, 2017; accepted August 30, 2017; published OnlineFirst September 6, 2017.

References

1. Foulkes WD, Smith IE, Reis-Filho JS. Triple-negative breast cancer. N Engl J Med 2010;363:1938–48.
2. Gusterson B. Do "basal-like" breast cancers really exist? Nat Rev Cancer 2009;9:128–34.
3. Metzger-Filho O, Tutt A, de Azambuja E, Saini KS, Viale G, Loi S, et al. Dissecting the heterogeneity of triple-negative breast cancer. J Clin Oncol 2012;30:1879–87.
4. Lehmann BD, Bauer JA, Chen X, Sanders ME, Chakravarthy AB, Shyr Y, et al. Identification of human triple-negative breast cancer subtypes and preclinical models for selection of targeted therapies. J Clin Invest 2011;121:2750–67.
5. Neve RM, Chin K, Fridlyand J, Yeh J, Baehner FL, Fevr T, et al. A collection of breast cancer cell lines for the study of functionally distinct cancer subtypes. Cancer Cell 2006;10:515–27.
6. Shah SP, Roth A, Goya R, Oloumi A, Ha G, Zhao Y, et al. The clonal and mutational evolution spectrum of primary triple-negative breast cancers. Nat Cell Biol 2012;486:395–9.
7. Stephens PJ, Tarpey PS, Davies H, Van Loo P, Greenman C, Wedge DC, et al. The landscape of cancer genes and mutational processes in breast cancer. Nature 2012;486:400–4.
8. Banerji S, Cibulskis K, Rangel-Escareno C, Brown KK, Carter SL, Frederick AM, et al. Sequence analysis of mutations and translocations across breast cancer subtypes. Nature 2012;486:405–9.
9. Petrocca F, Altschuler G, Tan SM, Mendillo ML, Yan H, Jerry DJ, et al. A genome-wide siRNA screen identifies proteasome addiction as a vulnerability of basal-like triple-negative breast cancer cells. Cancer Cell 2013;24:182–96.
10. Marcotte R, Sayad A, Brown KR, Sanchez-Garcia F, Reimand J, Haider M, et al. Functional genomic landscape of human breast cancer drivers, vulnerabilities, and resistance. Cell 2016;164:293–309.
11. Hsu TYT, Simon LM, Neill NJ, Marcotte R, Sayad A, Bland CS, et al. The spliceosome is a therapeutic vulnerability in MYC-driven cancer. Nature 2015;525:384–8.
12. Iwata M, Ozawa Y, Uenaka T, Shimizu H, Niijima J, Kanada RM, et al. E7107, a new 7-urethane derivative of pladienolide D, displays curative effect against several human tumor xenografts. Cancer Res 2004;64:691–1.
13. Matera AG, Wang Z. A day in the life of the spliceosome. Nat Rev Mol Cell Biol 2014;15:108–21.
14. Liu S. The network of protein-protein interactions within the human U4/U6.U5 tri-snRNP. RNA 2006;12:1418–30.
15. Nguyen THD, Galej WP, Bai X-C, Savva CG, Newman AJ, Scheres SHW, et al. The architecture of the spliceosomal U4/U6.U5 tri-snRNP. Nature 2015;523:47–52.
16. Agafonov DE, Kastner B, Dybkov O, Hofele RV, Liu WT, Urlaub H, et al. Molecular architecture of the human U4/U6.U5 tri-snRNP. Science 2016;351:1416–20.
17. Wan R, Yan C, Bai R, Wang L, Huang M, Wong CCL, et al. The 3.8 Å structure of the U4/U6.U5 tri-snRNP: insights into spliceosome assembly and catalysis. Science 2016;351:466–75.
18. Fan L, Lagisetti C, Edwards CC, Webb TR, Potter PM. Sudemycins, novel small molecule analogues of FR901464, induce alternative gene splicing. ACS Chem Biol 2011;6:582–9.
19. petrocca-tnbc-splicing [Internet]. San Francisco (CA): Github. c2017- [cited 2017 May]. Available from: https://github.com/hbc/petrocca-tnbc-splicing.
20. TNBC splicing [Internet]. Boston (MA): Harvard T.H. Chan School of Public Health, Bioinformatics. c2017- [cited 2017 May]. Available from http://bioinformatics.sph.harvard.edu/petrocca-tnbc-splicing/.
21. Subramanian A, Tamayo P, Mootha VK, Mukherjee S, Ebert BL, Gillette MA, et al. Gene set enrichment analysis: a knowledge-based approach for interpreting genome-wide expression profiles. Proc Natl Acad Sci 2005;102:15545–50
22. Warde-Farley D, Donaldson SL, Comes O, Zuberi K, Badrawi R, Chao P, et al. The GeneMANIA prediction server: biological network integration for gene prioritization and predicting gene function. Nucleic Acids Res 2010;38:W214–20.
23. Champions Oncology [Internet]. Champions Oncology, Inc.; c2017 [cited 2017 May]. Available from http://championsoncology.com/.
24. Xie J, Beickman K, Otte E, Rymond BC. Progression through the spliceosome cycle requires Prp38p function for U4/U6 snRNA dissociation. EMBO J 1998;17:2938–46.
25. Schütze T, Ulrich AKC, Apelt L, Will CL, Bartlick N, Seeger M, et al. Multiple protein–protein interactions converging on the Prp38 protein during activation of the human spliceosome. RNA 2016;22:265–77.
26. Patro R, Mount SM, Kingsford C. Sailfish enables alignment-free isoform quantification from RNA-seq reads using lightweight algorithms. Nat Biotechnol 2014;32:462–4.
27. Katz Y, Wang ET, Airoldi EM, Burge CB. Analysis and design of RNA sequencing experiments for identifying isoform regulation. Nat Meth 2010;7:1009–15.
28. Love MI, Huber W, Anders S. Moderated estimation of fold change and dispersion for RNA-seq data with DESeq2. Genome Biol 2014;15:31.
29. Croft D, O'Kelly G, Wu G, Haw R, Gillespie M, Matthews L, et al. Reactome: a database of reactions, pathways and biological processes. Nucleic Acids Res 2011;39:D691–7.
30. Gao H, Korn JM, Ferretti S, Monahan JE, Wang Y, Singh M, et al. High-throughput screening using patient-derived tumor xenografts to predict clinical trial drug response. Nat Med 2015;21:1318–25.
31. Laetsch TW, Liu X, Vu A, Sliozberg M, Vido M, Elci OU, et al. Multiple components of the spliceosome regulate Mcl1 activity in neuroblastoma. Cell Death Dis 2014;5:e1072.
32. Moore MJ, Wang Q, Kennedy CJ, Silver PA. An alternative splicing network links cell-cycle control to apoptosis. Cell 2010;142:625–36.

33. Sharova LV, Sharov AA, Nedorezov T, Piao Y, Shaik N, Ko MSH. Database for mRNA half-life of 19 977 genes obtained by DNA microarray analysis of pluripotent and differentiating mouse embryonic stem cells. DNA Res 2009;16:45–58.
34. Bonnal S, Vigevani L, Valcárcel J. The spliceosome as a target of novel antitumour drugs. Nat Rev Drug Discov 2012;11:847–59.
35. Yokoi A, Kotake Y, Takahashi K, Kadowaki T, Matsumoto Y, Minoshima Y, et al. Biological validation that SF3b is a target of the antitumor macrolide pladienolide. FEBS J 2011;278:4870–80.
36. Hong DS, Kurzrock R, Naing A, Wheler JJ, Falchook GS, Schiffman JS, et al. A phase I, open-label, single-arm, dose-escalation study of E7107, a precursor messenger ribonucleic acid (pre-mRNA) splicesome inhibitor administered intravenously on days 1 and 8 every 21 days to patients with solid tumors. Invest New Drugs 2013;32:436–44.
37. Eskens FALM, Ramos FJ, Burger H, O'Brien JP, Piera A, de Jonge MJA, et al. Phase I pharmacokinetic and pharmacodynamic study of the first-in-class spliceosome inhibitor E7107 in patients with advanced solid tumors. Clin Cancer Res 2013;19:6296–304.